

Contents lists available at [SciVerse ScienceDirect](http://SciVerse.ScienceDirect.com)

Chemical Engineering Research and Design

IChemE

journal homepage: www.elsevier.com/locate/cherd

Modeling for the catalytic coupling reaction of carbon monoxide to diethyl oxalate in fixed-bed reactors: Reactor model and its applications

Ya-Ping Zhu, Song Tu, Zheng-Hong Luo*

Department of Chemical and Biochemical Engineering, College of Chemistry and Chemical Engineering, Xiamen University, Xiamen 361005, China

ABSTRACT

A two-dimensional (2D) pseudo-homogeneous reactor model was developed to simulate the performance of fixed-bed reactors for catalytic coupling reaction of carbon monoxide to diethyl oxalate. Reactor modeling was performed using a comprehensive numerical model consisting of two-dimensional coupled material and energy balance equations. A power law kinetic model was applied for simulating the catalytic coupling reaction with considering one main-reaction and two side-reactions. The validity of the reactor model was tested against the measured data from different-scale demonstration processes and satisfactory agreements between the model prediction and measured results were obtained. Furthermore, detailed numerical simulations were performed to investigate the effect of major operation parameters on the reactor behavior of fixed bed for catalytic coupling reaction of carbon monoxide to diethyl oxalate, and the result shows that the coolant temperature is the most sensitive parameter.

© 2011 The Institution of Chemical Engineers. Published by Elsevier B.V. All rights reserved.

Keywords: Multiphase reactors; Mathematical modeling; Kinetics; Fixed-bed reactor; Catalytic coupling reaction

1. Introduction

As one of the most important alcoholic compounds, ethylene glycol (EG) is widely used in organic synthesis, particularly in the polyester, synthetic fibre and paint industry, etc. (Eugene and Andre, 2001; Shoaefar et al., 2007). Recently, a green process for the preparation of EG independent of petroleum described in Scheme 1 was developed based on coal (Li et al., 2005; Meng, 2003; Xu et al., 2008a) and it was first industrialized in China in 2009 (Qian, 2009). This green process is one of the promising methods to convert coal to high-value chemicals (UOPLLC, 2002). Its key part is the catalytic coupling reaction, which is shown in Eq. (1):



Eq. (1) shows that the coupling reaction is the synthesis of diethyl oxalate ((COOEt)₂, DEO, (COOC₂H₅)₂) from carbon monoxide (CO) and ethyl nitrite (EtONO, EN, C₂H₅ONO) over supported metal catalyst. On the other hand, catalytic

coupling reactions can be accomplished in various types of reactors, such as autoclave, fluidized-bed reactor, or fixed-bed reactor (Cheimarios et al., 2010; Dudukovic, 2010; Hillestad, 2010; Meng et al., 2004). The last one plays a very important part in the chemical industry and is certainly the most important at present (Nijemeisland and Dixon, 2004; Nikačević et al., 2009). In practice, for the catalytic synthesis of DEO and the further synthesis of EG reported in China, the selected reactor is fixed-bed (Qian, 2009; Xu et al., 2010).

On the other hand, it is well known that the economic viability of DEO conversion is determined by capital costs and average product price (Qian, 2009). In this respect, the manufacture of DEO is by far the most capital-intensive of a DEO conversion plant. Therefore, the catalytic coupling reaction of CO to DEO should aim at utilizing reaction materials as efficiently as possible, and selectivity considerations are then extremely important in the design of the catalytic coupling reaction section. To achieve an optimum performance for the complete process, the catalyst and the reactor should be comprehensively optimized (Wang et al., 2003). Obviously, due

* Corresponding author. Tel.: +86 592 2187190; fax: +86 592 2187231.
E-mail address: luozh@xmu.edu.cn (Z.-H. Luo).

Received 27 August 2011; Received in revised form 23 November 2011; Accepted 4 December 2011

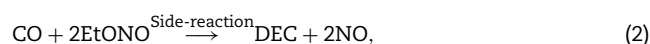
Nomenclature

a_1, a_2, b_1 and b_2	reactor model parameters
c_0	feed material mole concentration, mol/m ³
c_{CO}	the mole concentration of CO, kmol/m ³
c_p	heat capacity of raw material at constant pressure, kJ/(kg·K)
c_{pC}	heat capacity of coolant at constant pressure, kJ/(kg·K)
C_1	reactor model parameter
C_2, C_3	thermal conductivity parameters
d_p	catalyst Particle diameter, m
D	reactor diameter, m
Da	Dan Claire number
D_r	effective diffusion coefficient for raw materials, m ² /s
E_a	activation energy for the reaction, kJ/mol
f	pressure drop parameter of pressure drop
G	feed mass flux, kg/h
G_c	coolant mass flux, kg/h
h_{rs} and h_{rv}	model parameters of thermal conductivity, W/m ² K
k	pre-exponential factor mol/g h
k_g	mass transfer coefficient between gas and catalyst, m/h
L	length of tubular reactor, m
M_i ($i = CO, EN, ET, NO$ and N_2)	molecular weight of species i , g/mol
N	aspect ratio
P	operation pressure, MPa
Pr	Prandtl number
Pe_r	radial Peclet number
$(Pe_a)_m$	Peclet number along axial direction
Q_{in}	feed mole flux, mol/h
r	radial coordinate, m
R	universal gas constant kJ/kmol K
Re	Reynolds number
\mathcal{R}_i ($i = 1, 2, 3$)	reaction rate of the i th, kmol/kg h
S	cross sectional area of tubular reactor, m ²
S_p	surface area of catalyst particle per unit mass, m ² /kg
T	temperature, K
T_0	inlet temperature, K
T_c	coolant temperature, K
T_m	average temperature, K
u_0	inlet gas velocity, m/s
V	volumetric flow rate of feed, m ³ /s
x_i ($i = 1, 2, 3$)	EN conversion in the i th reaction, y_i mole fraction of specie i
$y_{i,0}$	inlet mole fraction of species i
z	axial coordinate, m
μ	viscosity, Pa s
μ_i	the viscosity of species i , Pa s
α, β	parameters of kinetic equations
λ	thermal conductivity of mixed gas, W m/K
λ_e	effective thermal conductivity in the radial direction, W m/K
λ_e^0	effective thermal conductivity in the radial direction for still fluid, W m/K
λ_s	effective thermal conductivity of catalyst, W m/K
ρ	density of gas mixture, kg/m ³

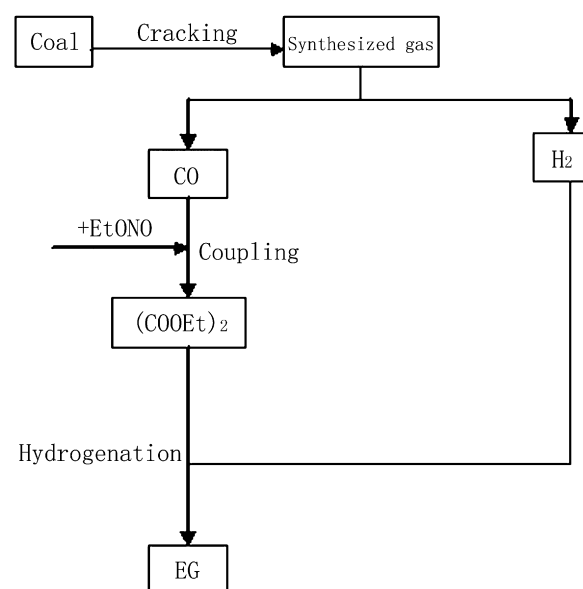
σ	parameter of thermal conductivity
ϕ, ϕ_1, ϕ_2	parameter of thermal conductivity
ε	porosity of bed
ΔP	pressure drop, kPa
ΔH_i ($i = 1, 2, 3$)	heat released of the i th reaction, kJ/mol

to the complexity of catalytic coupling reaction system, the proper establishment of pseudo-homogeneous reactor model, from which selectivity information as well as heat-transfer information can be derived in a quantitative fashion, is of critical importance.

There are many open reports on the coupling reaction of CO to DEO (Chatterjee et al., 2001; Gao et al., 2002, 2005; Ji et al., 2009; Le Gall et al., 2001; Meng et al., 2003, 2004; Wu et al., 2003; Xiao et al., 2000), most of them focused on the coupling reaction catalyst (Chatterjee et al., 2001; Gao et al., 2002, 2005; Ji et al., 2009; Le Gall et al., 2001; Wu et al., 2003; Xu et al., 1995) and mechanism (Ji et al., 2009; Meng et al., 2003, 2004; Xiao et al., 2000). Past studies (Chatterjee et al., 2001; Gao et al., 2002, 2005; Ji et al., 2009; Le Gall et al., 2001; Meng et al., 2003, 2004; Wu et al., 2003; Xiao et al., 2000) have proved that the coupling reaction process with fixed-bed reactors includes many reaction steps besides the main reaction step (Eq. (1)). Among them, there are mainly three reaction steps shown in Eqs. (1)–(3) which are paid attention (Gao et al., 2002, 2005; Le Gall et al., 2001; Meng et al., 2003, 2004; Wu et al., 2003; Xu et al., 1995):



where DEC is diethyl carbonate, ET is ethanol and AD is acetaldehyde. In addition, Eqs. (2) and (3) are the main side reactions. The coupling reaction is a highly exothermic reaction. In order to reduce pressure drop and facilitate heat removal, catalyst particles are generally needed to be used in fixed-bed reactors operating at high temperature. Accordingly,



Scheme 1 – A green process for the production of EG independent of petroleum.

the reaction system in fixed-bed reactors is a mixture of gas-phase and solid-phase. In order to develop the comprehensive modeling of the fixed-bed reactors, the reaction kinetics, mass and energy balance equations have to be solved together with considering the above side-reactions.

Up to now, reports on the coupling fixed-bed reactor model are relative few. Xu et al. (2008b) established a fixed-bed reactor model for the catalytic coupling reaction of CO to DEO with considering the above side-reactions. In their study, the gas concentration, temperature and pressure profiles along the axial direction inside the reactor were obtained. However, the usual assumption to model fixed-bed reactors of plug flow was still retained. Therefore, Xu et al.'s model (Xu et al., 2008b) is still one-dimensional model and the material selectivity cannot be obtained via their model. Wang et al. (2000a) developed a two-dimensional fixed-bed reactor model of coupling reactor of CO to DEO by using advanced software tools, Aspen and Pro-II. However, they ignored any side reaction. Due to ignoring the side reactions, Wang et al. (2000b) cannot obtain the special hot spots and their positions accurately via their two-dimensional model. In practice, when hot spots in reactor are considered, one cannot obtain the really hot spot temperature but an average temperature in selected reactor positions via a one-dimensional reactor model. In addition, the hot spot temperature obtained via the reactor model with ignoring any side reactions cannot reflect the practical situation very well as the side reactions is big enough to influence the simulated results. However, the hot spot temperature is important for catalyst's high temperature tolerance design and reactor optimization. A two-dimensional model including the side reactions can exactly solve the problems perfectly. In addition, in order to predict the raw material's selectivity, a two-dimensional model including side reactions works better than one-dimensional model, which is due to that the former one obtains the temperature distribution in the reactor more close to the real fact.

In this work, a two-dimensional pseudo-homogeneous reactor model based on two-dimensional coupled material and energy balance equations and incorporating a power law reaction kinetic model is developed to describe the performance of fixed-bed reactors for catalytic coupling reaction of CO to DEO, along with considering one main-reaction and two side-reactions. The reactor model is validated with the actual data collected from different-scale fixed-bed reactors. Furthermore, some reaction parameters in the reactor are obtained via the reactor model.

2. Simulated fixed-bed reactor and coupling reaction description

Since Li et al. (2004) and Xu et al. (2010) have experimentally investigated the coupling reaction of CO to DEO in a fixed-bed reactor and obtained many experimental data regarding the reaction, the fixed-bed reactor described in their work (Li et al., 2004; Xu et al., 2010) is selected as our simulated object. Referring to Refs. Li et al. (2004), Xu et al. (2010), the selected reactor has an inner diameter of 0.027 m and a length of 1.5 m. More detailed information regarding the reactor configuration is provided in Fig. 1. In addition, as to the fixed-bed reactor, the flow field in the reactor is calculated using a two-dimensional axis-symmetrical geometry.

On the other hand, as described earlier, the coupling reaction is the synthesis of DEO from CO and EN over supported metal catalyst (Pt/Al₂O₃) in the fixed-bed

reactor. In the fixed-bed reactor, the spherical catalyst particles of the same size are filled in the reactor. The gaseous EN and CO are continuously fed into the reactor, and react over the solid catalyst particles to produce gaseous DEO and a spot of by-products. In addition, in general, the catalysts carrying palladium catalyst particles are porous. Therefore, in this study, the reacting system is considered as a gas–solid two-phase system and the solid phase consists of porous catalyst particles and the involved reaction steps are listed in Eqs. (1)–(3). Consequently, the following reactor model is developed.

3. Development of reactor model

3.1. Reactor model assumptions

The utmost principle of the reactor model establishing procedures is to represent the actual reactor as accurate as possible under the conditions of necessary assumptions and simplifications, which, as a result, also helps the simulation to converge efficiently and steadily to a reliable result. Therefore, the following assumptions are made based on the above descriptions and Refs. Chen (2000), Li (2009), Meng et al. (2003), Wang et al. (2000b), Wu et al. (2003), Xu et al. (1995, 2008b, 2010):

(1) In practice, in our studied system, the gas velocity is great (0.83 m/s) and the catalyst particles is small (4 mm), heat and mass transfers between catalyst and fluid are strong enough. Namely, the difference of temperature and concentration between the solid phase and fluid phase can be ignored for a catalytic reaction (Li, 2009; Meng et al., 2003). Here, we also got the same result in Appendix A. It implies that a pseudo-homogeneous reactor model can be applied in this study.

(2) The tubular flow reactor was simulated with the conditions which are the same as the experiments. As the power law kinetics is fitted from the experiment data, which has included internal diffusion, we ignored it in present reactor model.

(3) The bed pressure drop calculated in Appendix A shows that it is really small. In this situation, the bed pressure drop has little effects on the reaction and reactor performance. In order to simplify the model, the bed pressure drop and momentum loss are negligible (Li, 2009; Wang et al., 2000b).

(4) The coupling reaction is performed in tubular flow reactors. Their structure parameters and operation conditions used in this study are listed in Table 1. Based on Table 1, one knows that the ratio of L/D is over 55. Therefore, the reaction can be assumed to behave as a plug flow reaction. This implies that the mass and heat diffusions in axial direction can be ignored (Chen, 2000; Li, 2009; Wang et al., 2000b). Here, we also got the same result in Appendix A.

3.2. Reaction kinetic model

With the fluid flows in the fixed-bed reactor, the coupling reaction takes place in the reactor. Therefore, the reaction kinetic model must be incorporated into the reactor model. Namely, the reactor model is completed by the kinetic equations (Shahrokhi and Baghmisheh, 2005). As described earlier, the porous palladium catalyst described in Li et al.'s work (2004) is selected in this study, and plus Li et al. (2004) also investigated the catalytic coupling reaction kinetics. Therefore, their kinetics is also applied in this study and is given below:

$$r_i = k \cdot e^{(-E_a/RT)} \cdot y_{CO}^\alpha \cdot y_{EN}^\beta \quad (4)$$

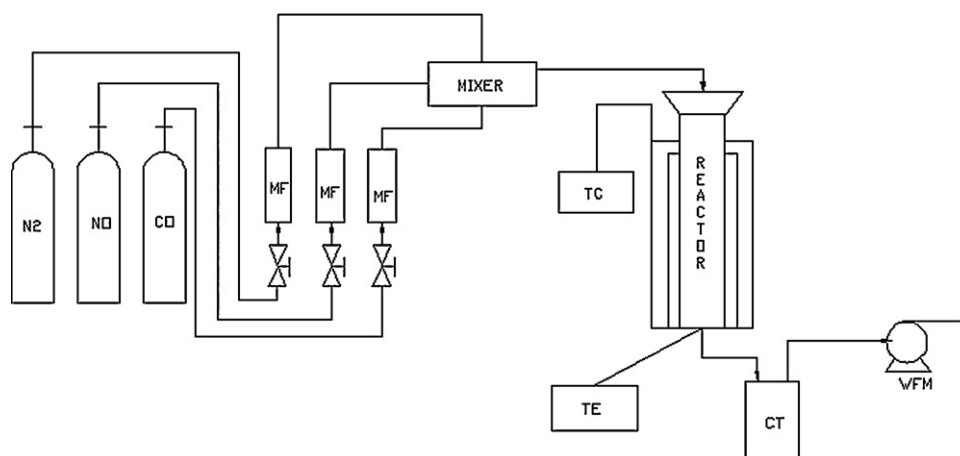


Fig. 1 – Experimental apparatus for the CO coupling reaction. (CT: cold trap; MF: mass flowmeter; TC: temperature control system; TE: thermocouple; WFM: wet flowmeter.)

Table 1 – The model parameters and comparisons between the experiment data and the simulation data.

Parameters	Values	Parameters	Values						
Operation pressure (Mpa)	0.2	Catalyst diameter (mm)	4.0						
Inlet temperature of the raw materials (K)	378	Temperature of coolant (K)	383						
Effective thermal conductivity of catalyst (kJ/m ² h K)	0.9	Void fraction of the reactor bed	0.4						
The parameters of the small-scale reactor									
Length (m)	0.015	Reactor diameter (m)	0.016						
The parameters of the pilot-plant reactor									
Length (m)	1.5	Reactor diameter (mm)	32 × 2.5						
Bulk density of the catalyst (kg/m ³)	980	Space velocity (h ⁻¹)	2000						
Mass flux of coolant (kg/h)	150	Scale (t/y)	300						
Model verification									
Material inlet mole flux (mol/h)	Inlet temperature (K)	CO inlet fraction	EN inlet fraction	DEO outlet fraction	DEC outlet fraction	ET outlet fraction			
				Actual	Calculated	Actual	Calculated	Actual	Calculated
The comparisons between the small scale reactor data and the simulation data									
0.4018	393	29.12%	11.49%	4.0282%	3.9338%	0.1655%	0.1869%	0.2050%	0.2333%
0.5357	393	24.16%	15.39%	3.3396%	3.3010%	0.1982%	0.2033%	0.3158%	0.3371%
0.6696	403	24.48%	17.20%	4.0189%	3.8392%	0.2460%	0.2226%	0.3147	0.4366%
The comparisons between the pilot-plant data and the simulation data									
79.717	378	24.7%	17.8%	7.32%	7.334%	0.181%	0.292%	-	0.892%
104.581	378	31.35%	10.63%	4.35%	4.322%	0.11%	0.177%	2.87%	2.93%

Table 2 – The kinetics parameters of reaction system.

The <i>i</i> th reaction	<i>k</i> (kmol/kg h)	<i>E_a</i> (kJ/kmol)	α	β
1	2.7551×10^4	4.4623×10^4	0.49	0.40
2	1.0815×10^2	2.6676×10^4	1.14	1.22
3	2.1832×10^4	4.6313×10^4	0	1.33

Eq. (4) is a power law function. It means that the applied kinetic model is a power law kinetic model. In addition, in Eq. (4), η_i ($i = 1, 2, 3$) is the reaction rate corresponding to the *i*th reaction step. Namely, $i = 1, 2$ and 3 correspond to Eqs. (1)–(3), respectively. Furthermore, the kinetic parameters corresponding to Eqs. (1)–(3) are listed in Table 2 (Li et al., 2004).

3.3. Reactor mathematical model

A two-dimensional (2D) pseudo-homogeneous model is chosen in this study to simulate the tubular fixed-bed DEO synthesis. The mass and energy equations for the differential

element volume in the selected reactor are given below (Chen, 2000; Li, 2009; Maestri et al., 2008; Wang et al., 2003).

Component mass balance:

$$\frac{\partial x_1}{\partial z} - a_1 \left(\frac{\partial^2 x_1}{\partial r^2} + \frac{1}{r} \frac{\partial x_1}{\partial r} \right) - b_1 \eta_1 = 0, \quad (5)$$

$$\frac{\partial x_2}{\partial z} - a_1 \left(\frac{\partial^2 x_2}{\partial r^2} + \frac{1}{r} \frac{\partial x_2}{\partial r} \right) - b_1 \eta_2 = 0, \quad (6)$$

$$\frac{\partial x_3}{\partial z} - a_1 \left(\frac{\partial^2 x_3}{\partial r^2} + \frac{1}{r} \frac{\partial x_3}{\partial r} \right) - b_1 \eta_3 = 0. \quad (7)$$

Energy balance:

$$\frac{\partial T}{\partial z} - a_2 \left(\frac{\partial^2 T}{\partial r^2} + \frac{1}{r} \frac{\partial T}{\partial r} \right) + b_2 (\Delta H_1 x_{r1} + \Delta H_2 x_{r2} + \Delta H_3 x_{r3}) = 0 \quad (8)$$

where x_i ($i = 1, 2, 3$) is the EN conversion corresponding to the i th reaction step, all a_1, b_1, a_2 and b_2 are model parameters and can be written as follows:

$$a_1 = \frac{d_p}{Pe_r} \quad (9)$$

$$b_1 = \frac{\rho}{u_0 c_0} \quad (10)$$

$$a_2 = \frac{\lambda_e}{Gc_p} \quad (11)$$

$$b_2 = \frac{\rho}{Gc_p} \quad (12)$$

Boundary conditions:

At the wall, the metal heat conductivity coefficient is much bigger than the effective thermal conductivity of catalyst. We consider the reactor temperature at the wall is equal to the coolant temperature. The coolant flows in the same direction with the fluid flow, so we can obtain Eq. (13) by heat balance while using infinitesimal method.

$$G_c \cdot c_{pc} \cdot \frac{\partial T}{\partial z} dz = G_c \cdot c_{pc} \cdot \frac{\partial T_c}{\partial z} dz = -\pi \cdot D \cdot dz \cdot \lambda_e \cdot \frac{\partial T}{\partial r} \Big|_{r=D/2} \quad (13)$$

Eq. (13) and other boundary conditions are rewritten as follows.

$$z = 0: T = T_0; x_i (i = 1, 2, 3) = 0 \quad (14)$$

$$r = 0: \frac{\partial T}{\partial r} = 0; \frac{\partial x_i}{\partial r} (i = 1, 2, 3) = 0 \quad (15)$$

$$r = D/2: \frac{\partial T}{\partial z} = -\frac{\pi D \lambda_e}{G_c c_{pc}} \frac{\partial T}{\partial z} \frac{\partial x_i}{\partial r} (i = 1, 2, 3) = 0 \quad (16)$$

Therefore, Eqs. (4)–(16) constitute the two-dimensional pseudo-homogeneous reactor model to simulate the tubular fixed-bed DEO synthesis from CO.

4. Model implementation and estimation of model parameters and actual data

Eqs. (4)–(16) include a set of coupled, linear partial differential and algebraic equations to simulate the performance of the tubular fixed-bed reactor. The partial differential equations (PDEs) were discretized simultaneously using the Crank–Nicholson finite-difference method subject to the boundary conditions (Forsythe and Wasow, 2004). Therefore, the PDEs were changed into linear algebraic equations. The resulting algebraic equations can be solved by LU method, but in our work a FSOLVE-function provided in Matlab 6.5 software was employed to solve those algebraic equations. The FSOLVE-function is a powerful program which is based on the least-squares method. In order to solve the suggested reactor model, some model parameters (including thermodynamic and physical property parameters) must be obtained in advance. The adopted thermodynamic and physical property parameters are listed in Table 3. In addition, some other

model parameters need to be estimated and their estimation are listed in Appendix A.

5. Results and discussion

5.1. Model verification

Since Li et al. (2004) and Xu et al. (2010) have obtained many experimental data regarding the fixed-bed reactor shown in Fig. 1, these experimental data are used to validate our suggested pilot-plant scale reactor model in this work. Furthermore, recently, Chen (2008) also obtained some experimental data from a small-scale fixed-bed reactor which is as well included in the validation.

Table 1 gives the small scale and pilot-plant scale reactor parameters related to the above reactor model, and the comparisons between the actual data collected from the small scale and pilot-plant reactors and the simulation results are also list in Table 1. Table 1 illustrates a good agreement between those data, which proves that the above model has the capability to simulate the performance of the fixed-bed reactors for catalytic coupling reaction of CO to DEO. In the next section, the above reactor model is only applied to simulate the performance of the pilot-plant scale reactor.

5.2. Flow field distribution

When the model is verified, it is firstly used to obtain the detailed flow field performance in the pilot-plant scale fixed-bed reactor. The reactor performance is described via the temperature, component conversion and/or mole fraction distribution profiles in the reactor at certain reaction condition. In addition, the following simulated conditions are as follows: $Q_{in} = 101.581$ mol/h, $T_0 = 378$ K, $T_c = 383$ K, $P = 0.2$ Mpa, $y_{CO,0} = 0.3135$, $y_{EN,0} = 0.1063$, $y_{NO,0} = 0.0047$, $y_{ET,0} = 0.0250$.

Fig. 2(a) shows the average temperature and EN conversion along the axial direction in the CO coupling reactor. According to Fig. 2(a), the EN conversion increases along the reactor due to reaction and it reaches 0.87 at outlet.

One can also learn from Fig. 2(a) that the axial temperature distribution in CO coupling reactor is well-proportioned, it goes up before the hot spot quickly and goes down slowly after the hot spot, which is due to rapid reaction rate and strong heat dissipation.

However, the radial temperature, which is shown in Fig. 2(b), changes shapely across the reactor, especially in the field near the hot spot. In addition, Fig. 2(b) also illustrates that the radial temperature in the reactor distribute as a n-type regularly. In practice, the above temperature changes are due to the thermal resistance and temperature gradient between the bed and the wall of the reactor. Compare Fig. 2(a) with Fig. 2(b), the maximum temperature have more than 10 K difference, which shows that 2D model obtain hot temperature more accurate than 1D model.

Fig. 3 shows the average mole fractions of materials in the system. From Fig. 3, the mole fractions of CO, EN, DEO and NO changes greatly, while compares with the other materials, and mole fraction of DEC and AD are very small. This is because the high conversion and selectivity of EN. The simulated EN selectivity is 88.75%. The ET mole fraction is bigger than that of DEC cross the reactor as ET is the main impurity in the raw materials.

Table 3 – The thermodynamic and physical property parameters.

Heat capacity (kJ/(kg·K))	$C_p = A + B \cdot T + C \cdot T^2 + D \cdot T^3$			
Materials	A	B	C	D
CO	27.487	4.248×10^{-3}	2.509×10^{-6}	-1.244×10^{-9}
EN	6.5618	2.9315×10^{-1}	-1.6311×10^{-6}	3.24×10^{-8}
NO	29.199	-7.8×10^{-4}	9.929×10^{-6}	-4.346×10^{-9}
N ₂	31.25	-1.361×10^{-2}	2.688×10^{-5}	-1.171×10^{-8}
DEO	123.59	1.9334	6.6506×10^{-4}	1.321×10^{-9}
DEC	74.690	1.4041×10^{-1}	5.7591×10^{-4}	6.4001×10^{-7}
Viscosity of reaction materials				
Materials	CO	EN	N ₂	NO
Viscosity $\times 10^6$ (Pa·s)	20.806	228	21.102	22.265
Heat of reactions				
The ith reaction	1	2	3	
Heat of reaction (kJ/kmol)	-135.2	-126.06	10.96	

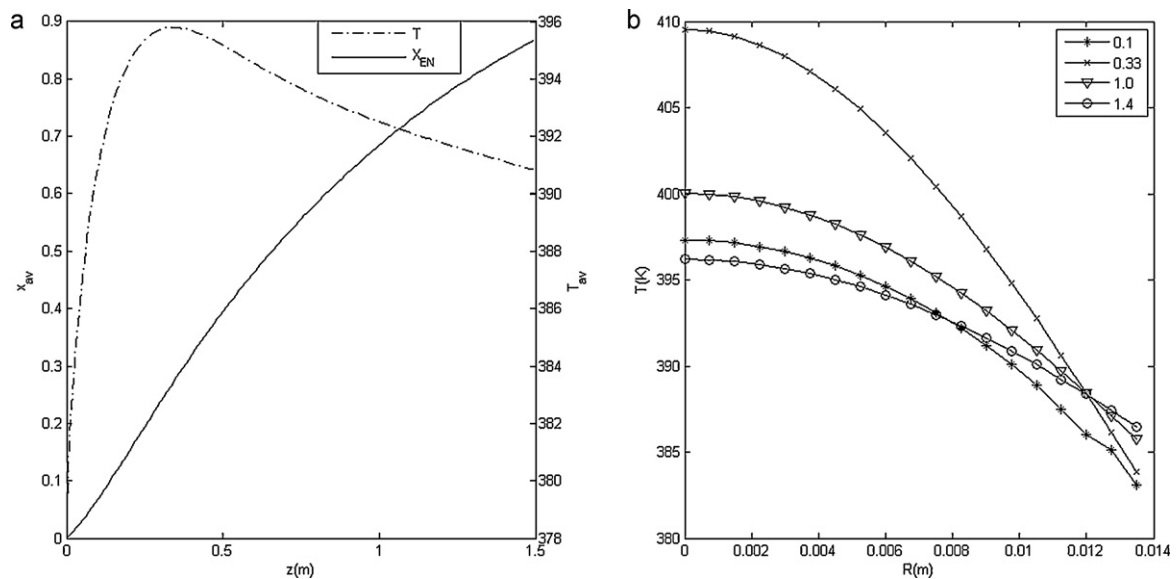


Fig. 2 – (a) The axial distributions of average reactor temperature and EN conversion in the reactor. (b) The radial temperature distributions at different bed positions ($Q_{in} = 101.581$ mol/h, $T_0 = 378$ K, $T_c = 383$ K, $P = 0.2$ MPa, $y_{CO,0} = 0.3135$, $y_{EN,0} = 0.1063$, $y_{NO,0} = 0.0047$, $y_{ET,0} = 0.0250$).

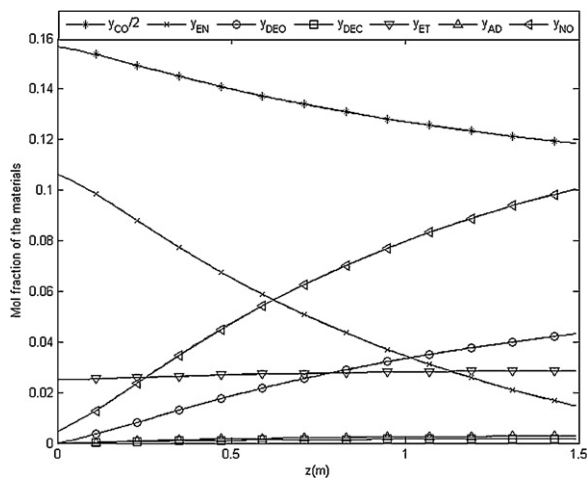


Fig. 3 – The materials' average mole fraction distribution along axial direction of the reactor ($Q_{in} = 101.581$ mol/h, $T_0 = 378$ K, $T_c = 383$ K, $P = 0.2$ MPa, $y_{CO,0} = 0.3135$, $y_{EN,0} = 0.1063$, $y_{NO,0} = 0.0047$, $y_{ET,0} = 0.0250$).

5.3. The effects of main operation parameters

The above model is also used to predict the effects of main operation parameters on the temperature in the reactor, i.e. the feed gas temperature, reactor coolant temperature, feed compositions and space velocity, on the reactor behavior of the pilot-plant scale fixed-bed reactor.

5.3.1. The effect of the feed gas temperature

The following simulated conditions are as follows: $y_{CO,0} = 0.25$, $y_{EN,0} = 0.15$, $y_{NO,0} = 0.04$, $y_{ET,0} = 0.025$, $T_c = 383$ K, $Q_{in} = 104.5813$ mol/h, $P = 0.2$ MPa. Correspondingly, the simulated results are shown in Fig. 4.

Fig. 4(a) shows the axial distributions of reactor temperature under different feed gas temperatures. From Fig. 4(a), when the feed temperature (i.e. 398 K and 408 K) is much higher than the coolant temperature, the temperature at the inlet section of the reactor will fluctuate and then fall slowly after the hot spot. In practice, it is well known that if the feed temperature is much higher, the reaction rate would be fast and the difference between the bed and the wall is big. Correspondingly, it leads to the high heat exchange rate and a shape temperature drop in the reactor bed. With the

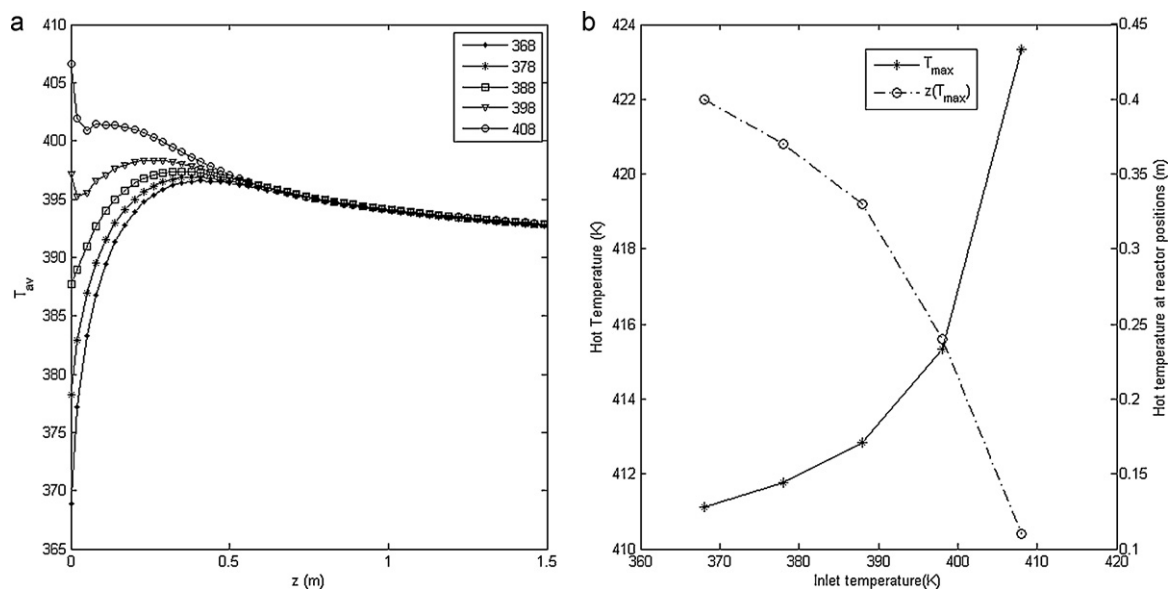


Fig. 4 – The effects of feed gas temperature. (a) The effect of feed gas temperature on the temperature distribution along axial direction of reactor. (b) The effect of feed gas temperature on the hot spot temperature and its position ($y_{CO,0} = 0.25$, $y_{EN,0} = 0.15$, $y_{NO,0} = 0.04$, $y_{ET,0} = 0.025$, $T_c = 383$ K, $Q_{in} = 104.5813$ mol/h, $P = 0.2$ MPa).

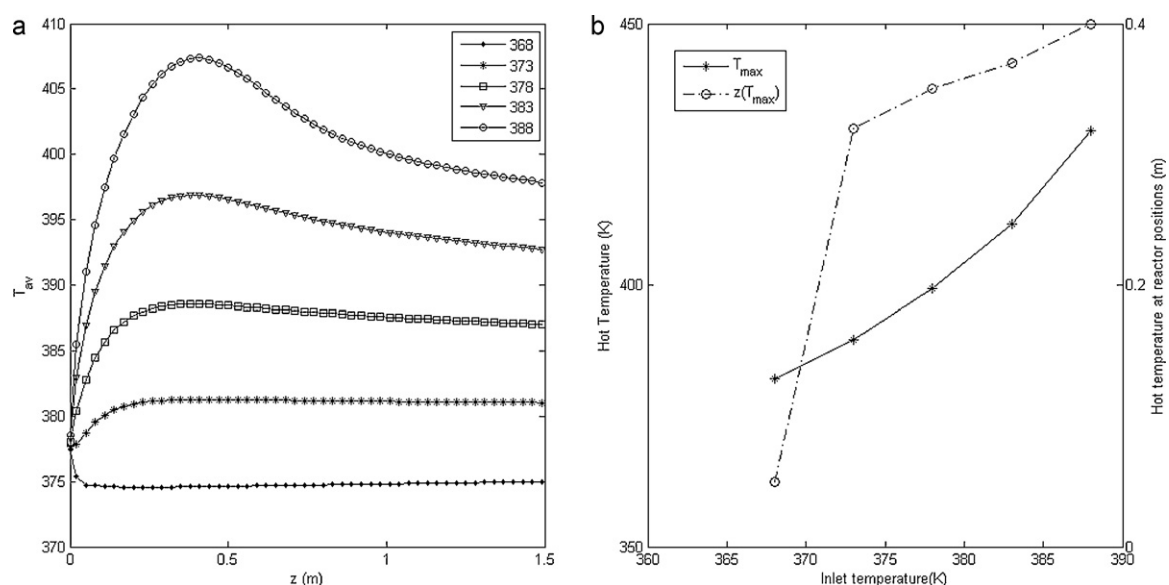


Fig. 5 – The effects of coolant temperature. (a) The effect of coolant temperature on the temperature distribution along axial direction of reactor. (b) The effect of coolant temperature on the hot spot temperature and its position ($y_{CO,0} = 0.25$, $y_{EN,0} = 0.15$, $y_{NO,0} = 0.04$, $y_{ET,0} = 0.025$, $T_0 = 378$ K, $Q_{in} = 104.5813$ mol/h, $P = 0.2$ MPa).

decrease of the reactor bed temperature, the heat exchange rate decreases, causing a rapid increase of the reactor bed temperature relatively. The bed temperature fluctuate do harms a steady operation. Accordingly, a high feed temperature is not recommended. In addition, Fig. 4(a) shows that high feed temperature leads to high temperature at the front part of the reactor, but the temperature at posterior are the same. One can find that the temperature at posterior is effected by coolant temperature rather than the feed temperature when combines with Fig. 5(a).

Fig. 4(b) gives the temperatures and positions of hot spot at different feed temperatures. From Fig. 4(b), the hot spot temperature increases rapidly when the feed temperature is higher than 398 K due to rapid reaction rate but un-effective dispel of heat. In addition, Fig. 4(b) indicates that the high feed temperature brings forward the hot spot. It is because the high

feed temperature leads to an increase of reaction rate and thus the forward of reaction zones.

On the other hand, considering the decrease of catalyst activity, the enduring of reactor and the pyrolysis of EN at high temperature, the feed temperature should be kept in a appropriate range and as high as possible for high yield of DEO. An adapted feed temperature is in the range of 368–388 K.

5.3.2. The effect of the coolant temperature

As the CO coupling reaction is a highly exothermic reaction, the temperature of heat exchange medium plays an important role in guaranteeing the steady temperature in the reactor. The following simulated conditions are as follows: $y_{CO,0} = 0.25$, $y_{EN,0} = 0.15$, $y_{NO,0} = 0.04$, $y_{ET,0} = 0.025$, $T_0 = 378$ K, $Q_{in} = 104.5813$ mol/h, $P = 0.2$ MPa. Fig. 5 showS the simulated results at different coolant temperatures.

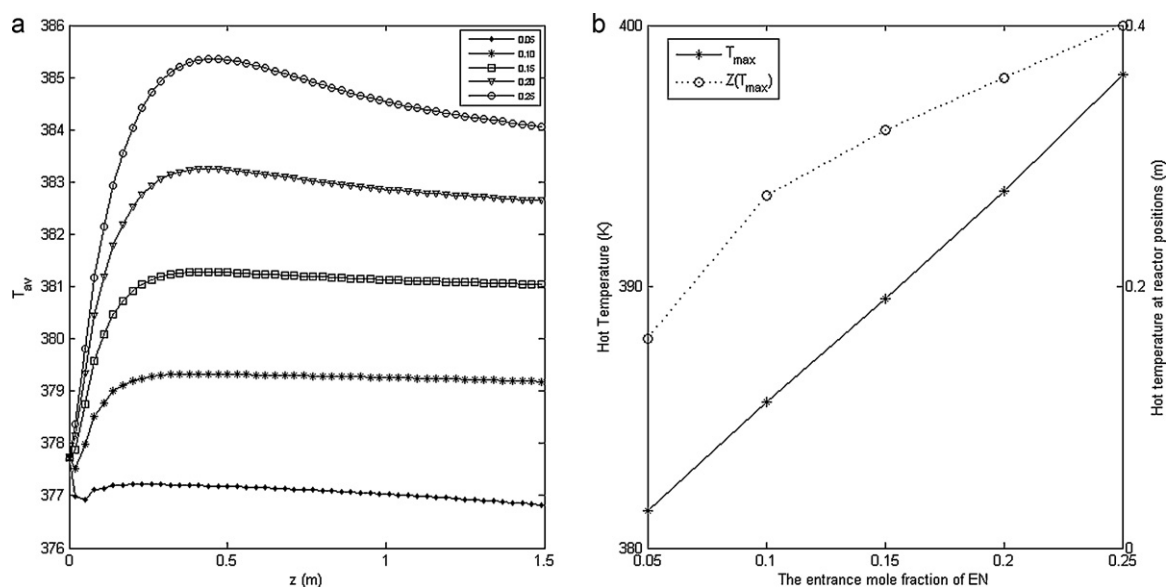


Fig. 6 – The effects of EN feed mole fraction. (a) The effect of EN feed mole fraction on the temperature distribution along axial direction of reactor. (b) The effect of EN feed mole fraction on the hot spot temperature and its position ($y_{CO,0} = 0.25$, $y_{NO,0} = 0.04$, $y_{ET,0} = 0.025$, $T_0 = 378$ K, $T_c = 373$ K, $Q_{in} = 104.5813$ mol/h, $P = 0.2$ MPa).

Fig. 5(a) describes the axial temperature distributions of reactor at different coolant temperatures. From Fig. 5(a), the reactor temperature climbs up with the ascending of coolant temperature. When the coolant temperature is much lower than the feed temperature, the reactor temperature at inlet section will fluctuate and the whole reactor temperature will keep at a low level due to the capability of heat exchange rate.

Fig. 5(b) indicates the high coolant temperature brings backwards the hot spot and a raise of the hot spot temperature. In practice, the high coolant temperature leads to a high reactor temperature. Such a high reactor temperature accelerates reaction rates and accumulates heat greatly until the accumulating heat rate equals the dispersal heat rate, resulting in high hot spot temperature and backwards-shifted hot spot position.

An appropriate coolant temperature is not higher than 378 K in order to keep a high reactor temperature and avoid the generation of many by-products (which is shown in Fig. 9) as well as the catalyst deactivation due to high hot spot temperature.

5.3.3. The effect of the EN feed mole fraction

The following simulated conditions are as follows: $y_{CO,0} = 0.25$, $y_{NO,0} = 0.04$, $y_{ET,0} = 0.025$, $T_0 = 378$ K, $T_c = 373$ K, $Q_{in} = 104.5813$ mol/h, $P = 0.2$ MPa. In order to keep the reactor in a reduction atmosphere and to restrain the EN reduction reaction, the EN feed mole fraction should be lower than that of CO. Therefore, the EN feed mole fraction becomes an important factor. Its effects are simulated and are shown in Figs. 6 and 7.

Fig. 6 gives the axial distributions of reactor temperature, the changes of hot spot temperature and position at different EN feed mole fractions, respectively. From Fig. 6, both the reactor temperature and hot spot temperature increase with the increase of EN mole fraction, which is due to that the high EN mole fraction leads to a rapid reaction rate, resulting in strong heat accumulation in very short time. As large amount of heat is generated in a time step, the heat accumulation in the reactor bed and the heat dissipation by the wall is strongly imbalanced, resulting in a much higher hot spot

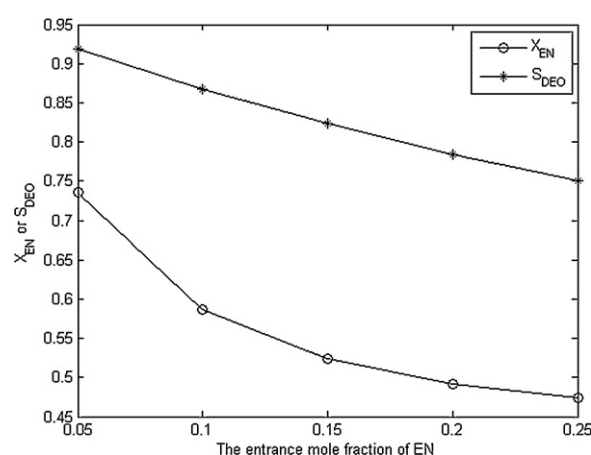


Fig. 7 – the effect of EN feed mole fraction on the EN conversion and DEO selectivity ($y_{CO,0} = 0.25$, $y_{NO,0} = 0.04$, $y_{ET,0} = 0.025$, $T_0 = 378$ K, $T_c = 373$ K, $Q_{in} = 104.5813$ mol/h, $P = 0.2$ MPa).

temperature and a backwards-shifted hot spot positions. In addition, Fig. 6(a) shows another important phenomenon that when the EN feed mole fraction is lower than 0.10 (i.e. 0.05, 0.10), the reactor temperature at the inlet of reactor will fluctuate and then stay in a low level, which could be explained by the wide temperature gap between the inlet section and the reactor wall caused by a low reaction rate.

Fig. 7 shows that the EN conversion decreases with the increases of EN feed mole fraction. It is because the EN mole fraction leads to incomplete reaction of EN, but the CO conversion increases with the increases of EN feed mole fraction, which is not shown in Fig. 7. In addition, Fig. 7 also illustrates that the EN selectivity drops with the increase of EN feed mole fraction. In practice, a high EN mole fraction means more EN take part in side reactions, resulting in the drops of EN selectivity. In short, an accept EN feed mole fraction is 0.15–0.20.

5.3.4. The effect of the space velocity

For the system with fixed volume and pressure, the reactor space velocity equals to the volume of raw materials

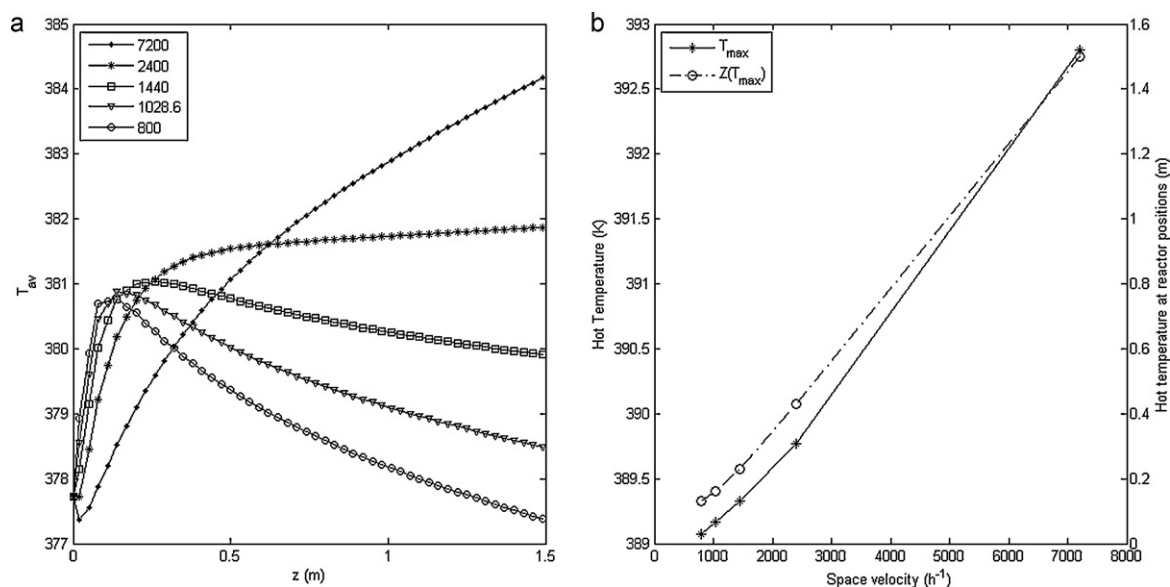


Fig. 8 – The effects of space velocity. (a) The effect of space velocity on the temperature distribution along axial direction of reactor. (b) The effect of space time velocity on the hot spot temperature and its position ($y_{CO,0} = 0.25$, $y_{EN,0} = 0.15$, $y_{NO,0} = 0.04$, $y_{ET,0} = 0.025$, $T_0 = 378$ K, $T_c = 383$ K, $P = 0.2$ MPa).

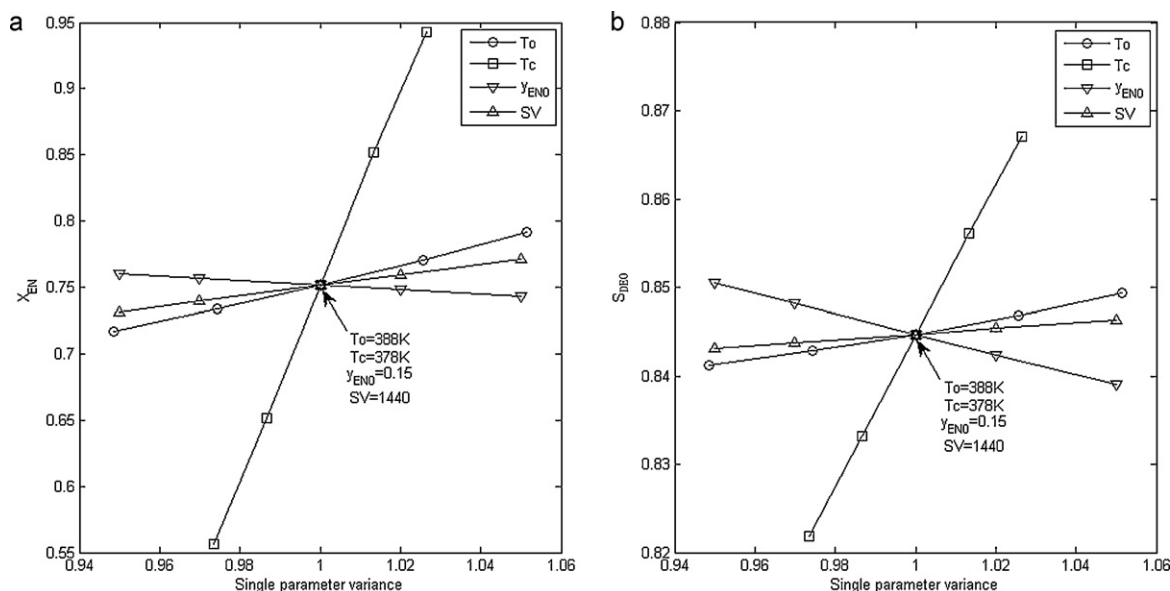


Fig. 9 – The EN conversion and DEO selectivity change by operation parameters.

per unit catalyst, the space velocity plays an important role to the CO coupling reaction. Correspondingly, the simulated results are shown in Fig. 8. The following simulated conditions is as follows: $y_{CO,0} = 0.25$, $y_{EN,0} = 0.15$, $y_{NO,0} = 0.04$, $y_{ET,0} = 0.025$, $T_0 = 378$ K, $T_c = 383$ K, $P = 0.2$ MPa.

Fig. 8(a) shows that the temperature runaway occurs at a high space velocity (i.e. $7200 h^{-1}$) due to a rapid reaction rate and strong heat accumulation. When the space velocity is low (i.e. $800 h^{-1}$), the raw material mole fractions stay in a low level, which leads to a low reaction rate, while the heat exchange is still great, resulting in a very low temperature in the outlet section of the reactor (i.e. 377 K).

Fig. 8(b) illustrates that the hot spot temperature increases and the position moves forward with the increase of space velocity. In practice, the low space velocity implies a small inlet gas volume flux and a little amount of raw materials, resulting in less reaction heat and lower hot spot temperature. In addition, the decrease of inlet gas volume flux leads to

a quick balance of heat exchange between the reactor bed and the reactor wall, resulting in the hot spot position's forward move.

In order to avoid the reactor temperature runaway, a space velocity between $1440 h^{-1}$ and $2400 h^{-1}$ would be appropriate.

5.4. Reaction analysis

EN is a main raw material in this system, but it is easy to take part in side reactions. While DEO is the target product, its selectivity is closely related with the economic benefits. The reactions, effected by operation parameters, are described by the conversion of EN and the selectivity of DEO, which are shown in Fig. 9. One can learn from Fig. 9 that the conversion of EN and the selectivity of DEO increase with the operation parameters, except the EN feed mole fraction, they have the same trend due to the strong competitiveness of the

main reaction. The coolant temperature is the most sensitive parameter.

6. Conclusions

A 2D pseudo-homogeneous reactor model was applied to simulate the catalytic coupling reaction of CO to DEO in a fixed-bed reactor based on the software MATLAB 6.5, using user defined functions to simulate and optimize the reactor model. Comparing the results gives the following conclusions:

- (1) The experiment data and simulated data show that the axial diffusion and the pressure drop can be ignored, while side reactions and radial direction transfer must be considered. The 2D pseudo-homogeneous reactor model is accurate enough to simulate the real reactor.
- (2) When compares with the feed gas temperature, the coolant temperature has much obvious effects on the reactor bed temperature and the hot spot in the coupling reactor. The simulated results show that both of them should not be too high in order to avoid a high hot spot temperature, and the gap between the feed gas temperature and the coolant temperature should be small in order to avoid the temperature oscillation in the inlet section of the reactor. In addition, it is much easier to control the bed temperature by changing coolant temperature.
- (3) The mole fraction of feed gas EN has obvious effect on the reactor temperature and EN selectivity due to its relatively low value. The simulated results show that the EN feed mole fraction would be accepted at a range of 0.15–0.20 in order to keep the reactor in a reduction atmosphere and to restrain the EN reduction reaction.
- (4) The simulated results show that the space velocity also has effect on the reactor temperature and EN conversion. To make reasonable choices of the space velocity, the DEO yield, EN selectivity and hot spot temperature must all be taken into consideration. A space velocity between 1440 h^{-1} and 2400 h^{-1} would be appropriate.

Acknowledgments

The authors thank the National Natural Science Foundation of China (No. 21076171), the State-Key Laboratory of Chemical Engineering (Tsinghua University) (No. SKL-ChE-10A03) and the Fujian Province Science and Technology Office of China (No. 2009HZ0005-1) for supporting this work.

Appendix A. Reactor model parameters

A.1. Axial dispersion

We consider a set of operation parameters which are as follows:

$\tau = 2000 \text{ h}^{-1}$; $P = 0.2 \text{ MPa}$; $y_{\text{CO}} = 0.25$; $y_{\text{NO}} = 0.06$; $y_{\text{N}_2} = 0.54$; $T_m = 383 \text{ K}$ (average temperature).

Then the Reynolds number in this system is 78.47. As described by Li (2009), the axial mass dispersion could be calculated as $(\text{Pea})_m = 2$ when the Reynolds number exceeds 50.

Aspect ratio is calculated by Eq. (A.1)

$$N = L/D = 1.5/0.027 = 55.56 > 55. \quad (\text{A.1})$$

When $(\text{Pea})_m = 2$ and $N > 55$, it is accurate enough to describe the real reactor by a plug flow model. In other words, the axial mass and axial heat dispersions can be ignored.

A.2. Radial Peclet number

Many experiments (Li, 2009) have made it clear that the radial Peclet number equals to 10 if the Reynolds number exceeds 20. Here, we assume the radial Peclet number is also 10.

A.3. Effective thermal conductivity in the radial direction

The radial effective thermal conductivity of fixed reactor is affected by the convection heat exchange of particle and fluid, the heat conduction of particle and fluid and the heat exchanged by radiation. The radial thermal conductivity can be calculated by Eq. (A.2):

$$\lambda e/\lambda = \lambda e^0/\lambda + (C_2 \cdot C_3) \cdot \text{Re} \cdot \text{Pr}, \quad (\text{A.2})$$

where e^0 is effective thermal conductivity in radial direction for still fluid and can be written as follows:

$$\lambda e^0/\lambda = \varepsilon(1 + h_{rv}d_p/\lambda) + \frac{1 - \varepsilon}{1/((1/\phi) + (h_{rs}d_p/\lambda)) + (2/3)(\lambda/\lambda_s)} \quad (\text{A.3})$$

in addition,

$$h_{rv} \text{ (W/m}^2 \text{ K)} = 0.227 \times \frac{1}{1 + \varepsilon/2(1 - \varepsilon)(1 - \sigma/\sigma)} \left\{ \frac{T_m}{100} \right\}^3, \quad (\text{A.4})$$

$$h_{rs} \text{ (W/m}^2 \text{ K)} = 0.227 \times \left(\frac{\sigma}{1 - \sigma} \right) \left(\frac{T_m}{100} \right)^3, \quad (\text{A.5})$$

$$\phi = \phi_2 + (\phi_1 - \phi_2) \frac{\varepsilon - 0.26}{0.216}, \quad (\text{A.6})$$

Therefore, the radial effective thermal conductivity can be obtained by Eqs. (A.3)–(A.6).

A.4. The reactor bed pressure drop

The pressure drop of the reactor bed can be estimated by Eq. (A.7).

$$\Delta P = f \frac{L u^2 \rho (1 - \varepsilon)}{d_p \varepsilon^3}, \quad (\text{A.7})$$

In our system, $P = 9.62 \text{ kPa}$, which means that the pressure drop of the coupling reactor is small (<15%) and the momentum lose can be ignored.

A.5. The external mass transfer

The mass transfer coefficient between gas and catalyst solid, k_g can be obtained by empirical formula, Eq. (A.8):

$$j_D = \frac{k_g \rho}{G} \left(\frac{\mu_{\text{CO}}}{\rho D_r} \right)^{2/3} = \frac{0.765}{\text{Re}^{0.82}} + \frac{0.365}{\text{Re}^{0.335}} \quad (\text{A.8})$$

And the Da number can be obtained by Eq. (A.9):

$$Da = \frac{\mathfrak{R}_{\text{CO,max}}}{k_g S_p c_{\text{CO}}} \quad (\text{A.9})$$

where $\mathfrak{R}_{\text{CO,max}}$ is the maximum reaction rate of CO. k_g is the mass transfer coefficient between gas and catalyst solid. S_p is

the surface area of catalyst particle per unit mass. c_{CO} is the mole concentration of CO. The Da is about 0.012 and the effective factor of external mass transfer is about 0.99 (Li, 2009; Meng et al., 2003), which means that the external transfer limitations can be ignored.

References

- Chatterjee, D., Deutschmann, O., Warnatz, J., 2001. Detailed surface reaction mechanism in a three-way catalyst. *Faraday Discuss.* 119, 371–384.
- Cheimarios, N., Kokkoris, G., Boudouvis, A.G., 2010. Multiscale modeling in chemical vapor deposition processes: coupling reactor scale with feature scale computations. *Chem. Eng. Sci.* 65, 5018–5028.
- Chen, B. B., 2008. Study on synthesis diethyl oxalate through CO coupling reaction. Master Dissertation, Tianjing University, Tianjing, China.
- Chen, G.T., 2000. *Chemical Reaction Engineering*. Chemical Industry Press, Beijing, China, pp. 184–200.
- Dudukovic, M.P., 2010. Reaction engineering: status and future challenges. *Chem. Eng. Sci.* 65, 3–11.
- Eugene, M.G., Andre, V.K., 2001. Carboxylates in catalytic hydrolysis of alkylene oxides. US Patent 6, 316, 571.
- Forsythe, G.E., Wasow, W.R., 2004. *Finite-difference Methods for Partial Differential Equations*. Dover Publications, New York, pp. 123–212.
- Gao, Z.H., Wu, Q., He, F., Li, Z.H., Xu, G.H., 2002. Study on ammonia poisoning of Pd system catalyst for CO coupling reaction to diethyl oxalate. *Chin. J. Catal.* 23, 95–98.
- Gao, Z.H., Liu, Z.C., He, F., Xu, G.H., 2005. Combined XPS and in situ DRIRS study of mechanism of Pd-Fe/ α -Al₂O₃ catalyzed CO coupling reaction to diethyl oxalate. *J. Mol. Catal. A: Chem.* 235, 143–149.
- Hillestad, M., 2010. Systematic staging in chemical reactor design. *Chem. Eng. Sci.* 65, 3301–3312.
- Ji, Y., Liu, G., Li, W., Xiao, W.D., 2009. The mechanism of CO coupling reaction to form dimethyl oxalate over Pd/ α -Al₂O₃. *J. Mol. Catal. A: Chem.* 314, 63–70.
- Le Gall, N., Luart, D., Salaun, J.Y., des Abbayes, H., Toupet, L., 2001. Mechanism of formation of the metallacyclic iron carbenes (CO)(3)Fe[=C(NR₂)OC(O)NR₂] formed by thermal evolution of bis carbamoyl complexes, characterization of eta(2)-carbamoyl intermediates. *J. Organomet. Chem.* 617, 483–494.
- Li, S.F., 2009. *Chemical and Catalytic Reaction Engineering*. Chemical Industry Press, Beijing, China, pp. 128–140.
- Li, Y.C., He, W.J., Fui, T.K., 2005. The method for production of ethylene glycol via direct catalytic hydrolysis of ethylene oxide over solid catalyst. CN Patent 1566049.
- Li, Z.H., He, C.Y., Xiang, T.L., Ma, X.B., Xu, G.H., 2004. CO coupling reaction to oxalate in gaseous phase over supported palladium catalysts. *Chem. React. Eng. Technol.* 20, 280–283 (in Chinese).
- Maestri, M., Beretta, A., Faravelli, T., Groppi, G., Tronconi, E., Vlachos, D.G., 2008. Two-dimensional detailed modeling of fuel-rich H₂ combustion over Rh/Al₂O₃ catalyst. *Chem. Eng. Sci.* 63, 2657–2669.
- Meng, F.D., 2003. Process analysis and simulation for the catalytic coupling reaction of carbon monoxide to diethyl oxalate. Ph.D. Dissertation, Tianjing University, Tianjing, China.
- Meng, F.D., Xu, G.H., Guo, R.Q., 2003. Kinetics of the catalytic coupling reaction of carbon monoxide to diethyl oxalate over Pd-Fe/ α -Al₂O₃ catalyst. *J. Mol. Catal. A: Chem.* 201, 283–288.
- Meng, F.D., Xu, G.H., Guo, R.Q., Yan, H.F., Chen, M.Q., 2004. Kinetic study of carbon monoxide coupling reaction over supported palladium catalyst. *Chem. Eng. Prog.* 43, 785–790.
- Nijemeisland, M., Dixon, A.G., 2004. CFD study of fluid flow and wall heat transfer in a fixed bed of spheres. *AIChE J.* 50, 906–921.
- Nikačević, N.M., Petkovska, M., Dudukovic, M.P., 2009. Solids flow pattern in gas – flowing solids – fixed bed contactors. Part II Mathematical modeling. *Chem. Eng. Sci.* 64, 2491–2500.
- Qian, B.Z., 2009. The industrialization of the preparation technology of ethylene glycol based on coal in China. *Petrochem. Technol. Appl.* 27, 360 (in Chinese).
- Shahrokhii, M., Baghmisheh, G.R., 2005. Modeling, simulation and control of a methanol synthesis fixed-bed reactor. *Chem. Eng. Sci.* 60, 4275–4286.
- Shoaeifar, P., Abbasian, M., Entezami, A.A., 2007. A convenient method for preparation of amphiphilic monomethoxypoly(ethylene glycol)-polystyrene diblock copolymer by NMRP technique. *J. Polym. Res.* 14, 45–52.
- UOPLLC, 2002. Attrition resistant catalyst for light olefin production. WO PCT 05952A2.
- Wang, B.W., Ma, X.B., Mao, L.F., Xu, G.H., 2000a. Simulation of the process of diethyl oxalate prepared by CO coupling-regeneration reaction. *J. Nat. Gas Chem.* 9, 187–196.
- Wang, B.W., Ma, X.B., Xu, G.H., Mao, L.F., 2000b. Optimization of cyclical process for CO coupling regeneration reactions. *Comput. Chem. Eng.* 24, 1337–1341.
- Wang, Y.N., Xu, Y.Y., Li, Y.W., Zhao, Y.L., Zhang, B.J., 2003. Heterogeneous modeling for fixed-bed Fischer-Tropsch synthesis: Reactor model and its applications. *Chem. Eng. Sci.* 58, 867–875.
- Wu, Q., Cao, Z.H., He, F., Xu, G.H., 2003. Influence of oxygen on activity of Pd-Fe/ α -Al₂O₃ catalyst for CO coupling reaction to diethyl oxalate. *Chin. J. Catal.* 24, 289–293.
- Xiao, W.J., Vasapollo, G., Alper, H., 2000. Highly regioselective thiocarbonylation of conjugated dienes via palladium-catalyzed three-component coupling reactions. *J. Org. Chem.* 65, 4138–4144.
- Xu, G.H., Ma, X.B., He, F., Chen, H.F., 1995. Characteristics of catalyst for carbon monoxide coupling reaction. *Ind. Eng. Chem. Res.* 34, 2379–2382.
- Xu, G.H., Ma, X.B., Wang, B.W., Li, Z.H., Zhang, Y.M., 2008. The method for production of diethyl oxalate via carbon monoxide coupling reaction. CN Patent 101143821.
- Xu, Y., Ma, X.B., Li, Z.H., 2008b. Simulation analysis on tube-shell type fixed bed reactor for synthesis of diethyl oxalate in gaseous phase. *Chem. React. Eng. Technol.* 24, 204–210 (in Chinese).
- Xu, Y., Li, R., Chen, M.M., Ma, X.B., 2010. Simulation of synthesizing diethyl oxalate by gaseous phase coupling carbon monoxide and ethyl nitrite. *J. Chem. Eng. Chin. Univ.* 24, 209–213.